Journal of
Marine Science and Engineering

MDPI

Article

Ultrasound Assisted Adsorptive Removal of Cr, Cu, Al, Ba, Zn, Ni, Mn, Co and Ti from Seawater Using Fe_2O_3-SiO_2-PAN Nanocomposite: Equilibrium Kinetics

Denga Ramutshatsha-Makhwedzha [1], Jane Catherine Ngila [1], Patrick G. Ndungu [1] and Philiswa Nosizo Nomngongo [1,2,3,*]

[1] Department of Chemical Sciences, University of Johannesburg, Doornfontein Campus, Johannesburg 17011, South Africa; denga.makhwedzha18@gmail.com (D.R.-M.); jcngila@uj.ac.za (J.C.N.); pgndungu@uj.ac.za (P.G.N.)
[2] DST/Mintek Nanotechnology Innovation Centre, Johannesburg 17011, South Africa
[3] DST/NRF SARChI Chair: Nanotechnology for Water, University of Johannesburg, Doornfontein 2028, South Africa
* Correspondence: pnnomngongo@uj.ac.za or nomngongo@yahoo.com; Tel.: +27-11-559-6187

Received: 6 March 2019; Accepted: 3 May 2019; Published: 9 May 2019

Abstract: This work reports the preparation and application of Fe_2O_3-SiO_2-PAN nanocomposite for the removal of Cr^{3+}, Cu^{2+}, Al^{3+}, Ba^{2+}, Zn^{2+}, Ni^{2+}, Mn^{2+}, Co^{2+}, and Ti^{3+} from seawater. X-ray diffraction (XRD), scanning electron microscope/energy dispersive X-ray spectroscopy (SEM/EDS), transmission electron microscope (TEM), and Brunauer-Emmett-Teller (BET) characterized the synthesized composite. The following experimental parameters (Extraction time, adsorbent mass and pH) affecting the removal of major and trace metals were optimized using response surface methodology (RSM). The applicability of the RSM model was verified by performing the confirmation experiment using the optimal condition and the removal efficiency ranged from 90% to 97%, implying that the model was valid. The adsorption kinetic data was described by the pseudo-second order model. The applicability of the materials was tested on real seawater samples (initial concentration ranging from 0.270–203 μg L^{-1}) and the results showed satisfactory percentage efficiency removal that range from 98% to 99.9%. The maximum adsorption capacities were found to be 4.36, 7.20, 2.23, 6.60, 5.06, 2.60, 6.79, 6.65 and 3.00 mg g^{-1}, for Cr^{3+}, Cu^{2+}, Al^{3+}, Ba^{2+}, Zn^{2+}, Ni^{2+}, Mn^{2+}, Co^{2+}, and Ti^{4+}, respectively.

Keywords: in-situ synthesis; Fe_2O_3-SiO_2-PAN nanocomposite; potential toxic metals; adsorption desalination; equilibrium kinetics

1. Introduction

Water crisis is the biggest problem faced by humanity and increased in water scarcity have a negative effect on economic development and human livelihoods [1]. The desire for clean water is caused by increase in global population, industrial activities, and development. Water scarcity can be resolved by means of building dams [2], use of ground water recharge [3], wastewater re-use [4] and desalination [5], among others, which are somewhat limited. However, the only endless resource that can produce high yield water is the ocean. The main concern about ocean water is that various types of contaminants around the globe are discharge in it. Then, this has affected the aquatic ecosystems and public health. This is motivating the search for a better technological solution to water shortage, whilst protecting ecosystem's health. Potential toxic metals (PTMs) are some of the pollutants that are

known to drive the reduction of marine life due to their toxic effects on living organisms [6]. This has also generated a huge interest amongst scientists and environmentalists in determining the global distribution of dissolved PTMs in the ocean.

Various methods such as chemical precipitation, ion exchange, biosorption, reverse osmosis and filtration have been used for removal of PTMs [7–10]. However, these methods are not commonly used because they are very expensive and their feasibility is extremely low [11,12]. On the other hand, adsorption technique remains an attractive method for removal of heavy metals due to its high removal efficiency and affordability [13,14].

Several scientists have conducted research on the development of cost effective and efficient use of the adsorbent for heavy metal removal. Therefore, metal oxides have been studied in depth for adsorptive removal of heavy metal. These include nanosized metal oxides (NMOs), which have good characteristics such as high surface areas and high activity [15–17]. Thus, α-Fe_2O_3 was found to be a more attractive alternative adsorbent to water treatment due to its cost-effectiveness and non-toxicity [18]. The nanostructures have a large surface area with excellent adsorption properties [19]. However, NMOs are unstable because of their nanoscale size, which leads to aggregation as a result of Van der Waals forces and later to the decrease in adsorption efficiency. In order to improve the stability state of NMO, their impregnation onto porous supports of natural materials, synthetic polymeric hosts and activated carbon has been reported [20]. These led to organic-inorganic polymer hybrids being used for its high transparency and excellent solvent-resistance [21].

Different methods have been used for preparation of different types of sorbents, these include the ex-situ and in-situ synthesis [22,23]. The use of in-situ synthesis has been the most used methods for the synthesis of polymers and nanoparticles to achieve homogeneous and well-dispersed material in polymer solution [24]. For this reason, preparation of composite materials such zeolitic imidazolate framework-8-PAN [23], sodium alginate-melamine sponge [25], poly (ether sulfone) (PES) and sulfonated poly (ether sulfone) (SPES) [26], and many others, were applied for heavy metal removal. Liu et al. (2011) showed that the uptake of As (III) was successfully accomplished using As (III) imprinted α-Fe_2O_3-impregnated chitosan beads [19]. Park et al. (2017) successfully impregnated Fe-Ti bimetal oxides into polymeric beads with the overall metal content of 4–6 wt.% [27].

Recently, the use of ultrasound irradiation has gained more attention in various applications [16,28–31]. This is because ultrasound assists in speeding the chemical process through the formation of acoustic cavitation, which is due to the propagation of pressure waves through liquid [28]. The process creates growth and collapse of the micrometer scale bubbles formed by pressure wave, which helps in strengthening mass transfer process. This, in turn, facilitates the interaction between adsorbate (major and trace metal ions) and adsorbent, thus leading to enhanced adsorption process [30,31]. In addition, shock waves have the ability of forming microscopic turbulence within the interfacial films that surrounds the solid particle [29]. Furthermore, this helps in accelerating interaction between the adsorbent and adsorbate (major and trace metals), thus reducing the time required to reach the equilibrium process [30,31].

In this study, a Fe_2O_3-SiO_2-PAN nanocomposite was applied for the first time as an adsorbent for treatment of PTMs in synthetic saline water samples and seawater. Where the synthesis of Fe_2O_3-SiO_2-PAN composite material was achieved through an in-situ process. Iron oxide was selected for this study because it is a cheap material that can be employed for easy separation, with large surface area and specific affinity [32,33]. Meanwhile, mesoporous silica has recently attracted huge interest as a suitable adsorbent for the removal of various pollutants due to its unique physicochemical properties [34]. These include properties such as possible re-use, mechanical resistance, and easy modification. In addition, an inert silica coating on the surface of magnetite nanoparticles prevent their aggregation in liquid substances or matrix [35]. Therefore, many research studies have applied functionalized silica as an adsorbent in the analysis of various metals and compounds [36–38]. However, it has been reported that inorganic adsorbents tend to cause operational problems such as clogging of filter membranes [39]. Therefore, incorporation of polymer matrix in the inorganic adsorbents has been found to act as inert organic binder for the removal of PTMs in complex matrices [39]. In this

study, the polymer of choice was polyacrylonitrile (PAN because of its cost effectiveness and attractive properties [40,41]. Some of its attractive properties include excellent molding to pellet property, low density, strong attractive forces with inorganic materials, and chemical and mechanical stability [39,42]. Thus, composite material Fe_2O_3-SiO_2 is an excellent candidate for producing composite fibers along with PAN due to their combined properties such as chemical stability and flexibility, among others. The combination of these materials presents a novel class of composite nanofibers that entails unique advantages as compared to other sorbents material used before. The following experimental parameters (Extraction time, adsorbent mass and pH) affecting the removal of Cr^{3+}, Cu^{2+}, Al^{3+}, Ba^{2+}, Zn^{2+}, Ni^{2+}, Mn^{2+}, Co^{2+}, and Ti^{3+} were optimized using a multivariate approach, namely a response surface methodology (RSM) based on the Box-Behnken design.

2. Experimental

2.1. Materials and Reagents

Ultra-pure water (Direct-Q® 3UV-R purifier system, Millipore, Merck, Germany) was used in these experiments. Tetraethyl orthosilicate (TEOS), ammonium hydroxide (NH_4OH) (25%, *w/v*), methanol (99.9%, HPLC grade), absolute ethanol, polyacrylonitrile (PAN, average Mw 150,000), N, N-dimethylformamide (DMF), tween-80 and sodium hydroxide, nitric acid (HNO_3) and ferric nitrate ($Fe(NO_3)_3$ $9H_2O$) were purchased from Sigma-Aldrich (St. Louis, MO, United States). A multi element standard solution of 100 mg L^{-1} containing the following elements of interest, (Al, Ba, Cd, Ca, Cr, Co, Cu, Fe, Pb, Mg, Mn, Ni, Na, Ti, and Zn) was supplied by Spex CertiPrep (Industrial Analytical (Pty) Ltd., Johannesburg, South Africa). The multi-elemental standard was also utilized for preparation of calibration standards. The pH of the model solutions was adjusted with 1.0 mol L^{-1} HNO_3 and NH_4OH.

2.2. Instrumentation

The oven (CEM Corporation Mars 6, Matthews, NC, USA) was used as drying source for the synthesis of the material. The inductively coupled plasma atomic emission spectroscopy (ICP-OES) (iCAP 6500 Duo, Thermo Scientific, UK) was used for quantification of analytes in sample solutions. The crystallinity of the material was studied by X-ray diffraction (XRD) analysis using PANalytical X'Pert X-ray Diffractometer and Cu Kα radiation spectrometer and the scanning area covered the range 2-theta at start position 4.00–80.00. The scanning electron microscopy (SEM) (HITACHI COM-S-4200) was used to study the morphology of the material. The Energy Dispersive X-ray (EDX) spectroscopy was connected to the SEM for determination of the ratio of Si/Fe. Jeol JEM-2100F field emission electron microscopy instrument (JEOL Inc, Akishima, Japan) was used for transmission electron microscopy (TEM) studies. The preparation of TEM samples was done by putting a small quantity of synthesized sample that has been dispersed into copper grid with carbon film. The surface area was analyzed using BET micrometric ASAP 2020.

2.3. Synthesis of Fe_2O_3-SiO_2 by Sol Gel Method

The preparation, of Fe_2O_3-SiO_2 was adopted from Ref [43] with some modifications. Mesoporous Fe_2O_3-SiO_2 composite was prepared by TEOS and ferric nitrate $Fe(NO_3)_3{\cdot}9H_2O$ respectively. The 300 mL of deionized water was mixed with 380 mL of absolute ethanol and stirred for 15 min for the preparation of mesoporous Fe_2O_3-SiO_2 composite. The 23.5 g of TEOS (98%) was added to the resulting solution and vigorously stirred for 30 min. Then, to the above clear solution, 4.6 g of $Fe(NO_3)_3{\cdot}9H_2O$ (Si/Fe = 50, respectively) was added at once and stirred for 30 min. For gelation to take place 115 mL of ammonium hydroxide was added and the formed precipitate was stirred for another 30 min and aged for 24 h at 25 °C. The material was then dried in an oven at a temperature of 60 °C for 24 h and calcined at 550 °C for 4 h in a furnace. The final product was cooled at room temperature and stored for further use.

2.4. Preparation of Fe_2O_3-SiO_2-PAN Nanocomposite

Fe_2O_3-SiO_2-PAN adsorbent was prepared following the procedure reported by İnan and Altaş [39]. Fe_2O_3-SiO_2 hydrous oxide powders synthesized were used in the experiment as inorganic active ion exchangers in the organic-inorganic composite beads. The prepared Fe_2O_3-SiO_2-PAN was composed of about 65 wt.% of Fe_2O_3-SiO_2 on a PAN polymeric support. A mass (10 g) of Fe_2O_3-SiO_2 hydrous powder was mixed with 50 mL of DMF (N, N-dimethylformamide) and a few drops of Tween-80 surfactant was stirred at a temperature of 50 °C for 2 h to form homogeneous solution. Then 2 g of PAN were added in the stirring solution and temperature was kept at 50 °C for 2 h to obtain homogeneous solution of the composite dope. Ultra-pure water/methanol alcohol mixture at a ratio of 2:1 was used as a gelation agent. The gelled composite beads were left 24 h for aging and washed using ultra-pure water. Modification was done on the surface of the spheres by 1 M NaOH and then washed and air-dried at 70 °C for 2 days to remove the solvent. The adsorbent was characterized using-ray diffraction (XRD), scanning electron microscope/energy dispersive X-ray spectroscopy (SEM/EDS), transmission electron microscope (TEM), and Brunauer-Emmett-Teller (BET).

2.5. Optimization of the Adsorption Batch Method

The optimisation method of the experimental conditions was performed using the Box-Behnken design matrix on the following factors: pH, extraction time (ET) and mass of adsorbent (MA). The minimum and maximum levels of the factors were generated and are shown in Table 1. The results were evaluated using the recovery of Co and similar results were obtained for all the metals.

Table 1. Variables and levels used in Box–Behnken design.

Variables	Low Level (−)	Central Points (0)	High Level (+)
pH	3.00	6.00	9.00
Extraction time (ET) (min)	5.00	17.5	30.0
Mass of adsorbent (MA) (mg)	100	200	300

2.6. Ultrasound Assisted Adsorptive Removal

In these experiments, 20 mL of Cr^{3+}, Cu^{2+}, Al^{3+}, Ba^{2+}, Zn^{2+}, Ni^{2+}, Mn^{2+}, Co^{2+}, and Ti^{3+} solution contained in 100 mL plastic bottles were contacted with 100 to 300 mg of Fe_2O_3-SiO_2-PAN nanocomposite adsorbent. The latter were then placed in a sample rack that was then dipped in an ultrasonic water bath at a temperature of 25 °C. Equilibrium adsorption studies on removal of Cr^{3+}, Cu^{2+}, Al^{3+}, Ba^{2+}, Zn^{2+}, Ni^{2+}, Mn^{2+}, Co^{2+}, and Ti^{3+} metals ions using ultrasonic assisted adsorptive removal method was performed in an ultrasonic bath for 5–20 min. The appropriate amount of supernatant was collected from the sonicated samples, filtered and analyzed using ICP-OES. This same procedure was performed for removal and treatment of PTMs in real samples. The adsorption capacity (Qe, mg g^{-1}) was calculated using Equation (2).

2.7. Application to Real Samples

Adsorption of Cr^{3+}, Cu^{2+}, Al^{3+}, Ba^{2+}, Zn^{2+}, Ni^{2+}, Mn^{2+}, Co^{2+} and Ti^{4+} in seawater was investigated and, experiments were conducted using the optimum conditions obtained from the RSM. Real water (seawater) samples collected from Durban, South Africa, were used to evaluate the applicability of adsorption method. The collected seawater samples were stored in lab plastic bottles for further analysis at a temperature of 4 °C, whilst pH and conductivity were found to be 8.3 and 47.7 mS/cm, respectively. The batch adsorption experiments of seawater samples were carried out using the optimum conditions and the procedure elaborated in Section 2.6 was used.

2.8. Data Analysis

The adsorption efficiency was calculated using Equation (1).

$$Adsorption\ efficiency = \frac{C_o - C_e}{C_o} \times 100 \quad (1)$$

where C_o is the initial concentration in mg L^{-1} and C_e is the final concentration mg L^{-1}.

The adsorption capacity that is the amount of metal ions adsorbed per gram adsorbent (mg g^{-1}). Its equation can be written as follows:

$$Adsorption\ capacity = \frac{C_o - C_e}{m} v \quad (2)$$

where C_o is the initial concentration in mg L^{-1}, C_e is the final concentration mg L^{-1}, m is the amount of the adsorbent in grams (g) and v is the volume of the sample solution measured in liters (L).

3. Results

3.1. Surface Identification and Characterisation

Prior to analysis, the prepared samples were finely crushed to powder, mounted in the sample holder and loaded in the sample rack analysis. The XRD analysis of Fe_2O_3-SiO_2 and Fe_2O_3-SiO_2-PAN are demonstrated in Figure 1. X-ray diffraction patterns ware analyzed by scanning from 4.00–80.00° 2-theta range. Figure 1a shows XRD patterns of SiO_2-Fe_2O_3 with crystalline structure of Fe_2O_3 at 2-theta values 35.3°, 44.7°, 56.1°, and 63.8°. These major characteristic peaks can be indexed as 104, 113, 116, and 300 according to the peak list obtained from the XRD report data. According to Debye-Scherer's equation the particle sizes for Fe_2O_3-SiO_2 nanocomposite ranged from 50–110 nm. These results are in agreement with the pattern reported by Panda et al. [43]. In addition, this crystalline structure was found to be monoclinic. When the polymer was introduced on the same material, an amorphous structure can be observed on the XRD pattern of Fe_2O_3-SiO_2-PAN (Figure 1b). Liu et al. [19] reported these observations.

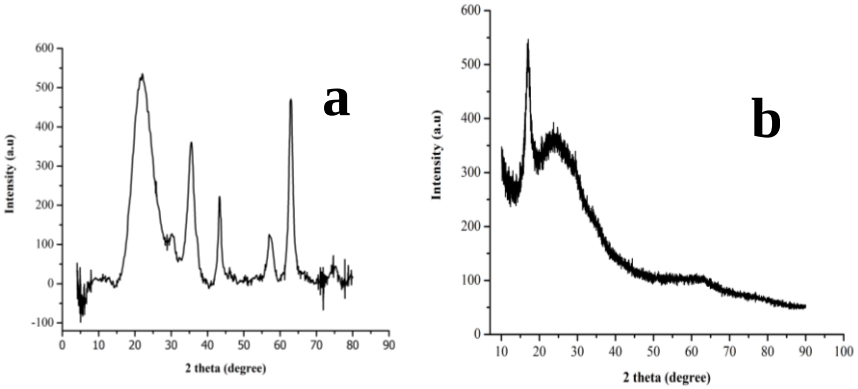

Figure 1. XRD patterns of (**a**) Fe_2O_3-SiO_2 and (**b**) Fe_2O_3-SiO_2-PAN.

Figure 2 shows the SEM images of Fe_2O_3-SiO_2 and Fe_2O_3-SiO_2-PAN composite that was studied through the SEM/EDX. The SEM image in Figure 2b shows the random distribution of large sizes that have irregular shapes through the encapsulation of Fe_2O_3-SiO_2 particles by PAN. Bhaumik et al. [44], reported results with the same resemblance. These observations were different from the images observed in Figure 2a, which confirms the incorporation of PAN.

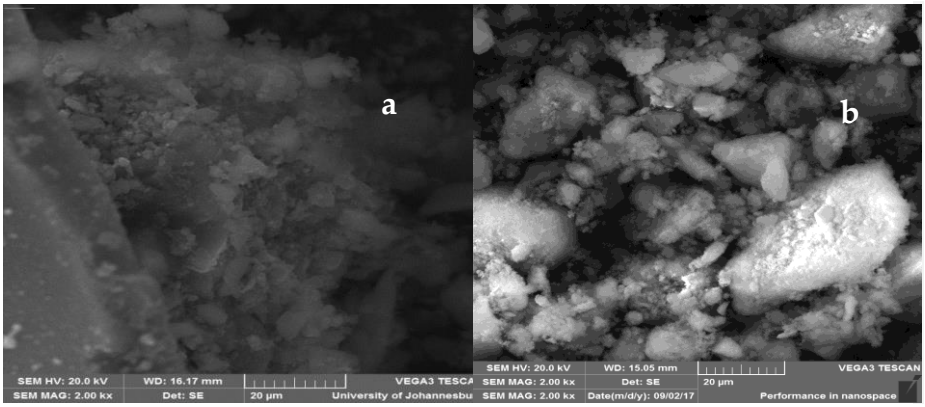

Figure 2. SEM images of (**a**) Fe_2O_3-SiO_2 (**b**) Fe_2O_3-SiO_2-PAN.

The TEM images of Fe_2O_3-SiO_2 and Fe_2O_3-SiO_2-PAN are shown in Figure 3. The Fe_2O_3-SiO_2 (Figure 3a) shows structures like hexagonal in shape. It is clear that Fe_2O_3-SiO_2 nanoparticles are incorporated on the surface of PAN. This is evident based on the distinctive film of PAN surrounding black spots that represent Fe_2O_3-SiO_2 nanocomposite. These results were further confirmed by EDX mapping densely covered Fe_2O_3-SiO_2 spheres. Setshedi et al. [45] and Teo et al. [46] reported similar observations.

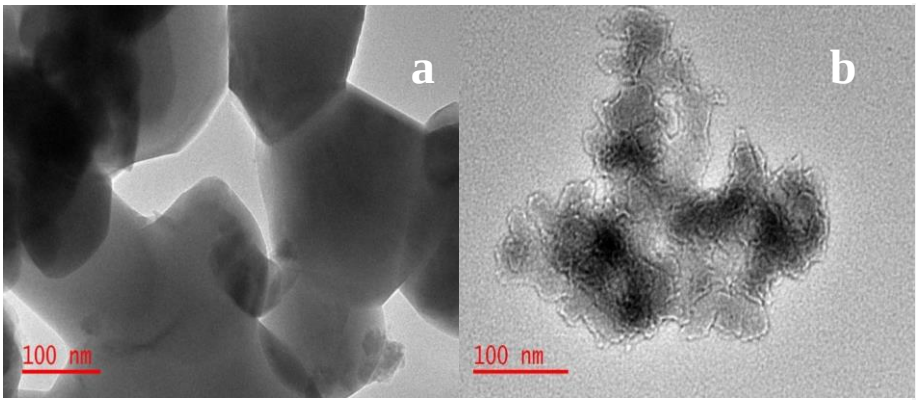

Figure 3. TEM image of (**a**) Fe_2O_3-SiO_2 (**b**) Fe_2O_3-SiO_2-PAN.

Figure 4 shows the SEM-EDS spectra of the prepared Fe_2O_3-SiO_2 and Fe_2O_3-SiO_2-PAN composites. The prepared composite material shows the presence of carbon (38%) compared to Fe_2O_3-SiO_2. The appearance of carbon in the spectrum of Fe_2O_3-SiO_2-PAN composite (Figure 4B) confirms the presence of PAN. The presence of carbon in Fe_2O_3-SiO_2 nanocomposite (Figure 4A) and Au in Fe_2O_3-SiO_2-PAN composite (Figure 4B) was a result of carbon and gold coating.

The dispersion of C, N, Fe, Si and O atoms was further investigated by EDX-mapping analysis (Figure 5). As seen in Figure 5, the composite composed of the expected elements that is C, N, Fe, Si, and O. The Fe_2O_3-SiO_2 nanoparticles were uniformly deposited on the surface of PAN.

The physical property analyses of Fe_2O_3-SiO_2 nanocomposite gave some understanding on the effect of cross-linking reaction to the chemical and physical properties of Fe_2O_3-SiO_2-PAN. The BET results are very important in explaining adsorption capacity of the adsorbents towards adsorbates. Data obtained from BET surface area analysis on Fe_2O_3-SiO_2 and Fe_2O_3-SiO_2-PAN were presented in Table 2. The surface areas of Fe_2O_3-SiO_2 and Fe_2O_3-SiO_2-PAN were 253 and 158 $m^2\ g^{-1}$, respectively. The reduced surface area on the composite may be due to the polymer layer shrinking around the nano-metal oxides matrix (Figure 3b).

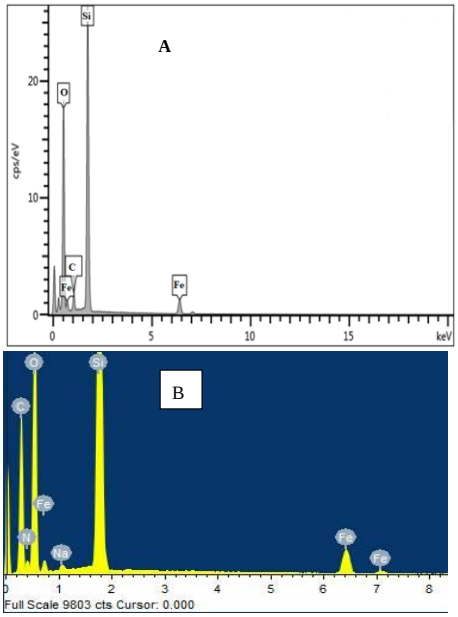

Figure 4. SEM-EDS spectra of (**A**) Fe_2O_3-SiO_2 nanocomposite and (**B**) Fe_2O_3-SiO_2-PAN.

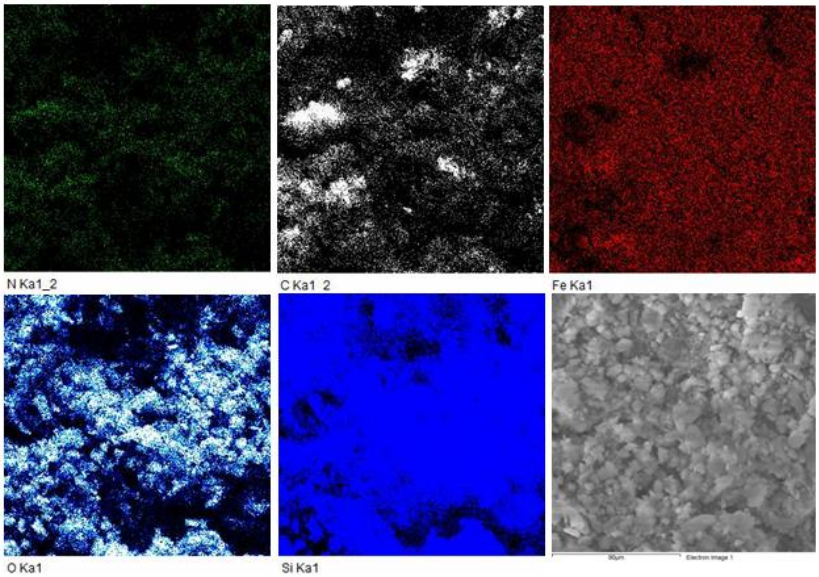

Figure 5. SEM-EDX mapping on Fe_2O_3-SiO_2-PAN.

Table 2. Summary of BET analysis.

Materials	Surface Area (m^2 g^{-1})	Pore Volume (cm^3 g^{-1})	Pore Size (nm)
Fe_2O_3-SiO_2	253	0.96	14.4
PAN	32.0	0.26	35.4
Fe_2O_3-SiO_2-PAN	158	0.53	22.1

Liu et al. (2011) showed that the internal pore structure of each material plays an important role in the adsorption performance of different adsorbate [19]. For this reason, the average pore diameter of Fe_2O_3-SiO_2 and Fe_2O_3-SiO_2-PAN were investigated and results were shown in Table 2. The pores are divided in comprehensive terms according to the size of their diameter (d) (IUPAC classification). Results show that both Fe_2O_3-SiO_2 and Fe_2O_3-SiO_2-PAN are mesopores in nature ($2 < d < 50$ nm). Therefore, Fe_2O_3-SiO_2-PAN composite could be a suitable adsorbent for the removal of PTMs. In addition, Munonde et al. [47], reported that nanocomposite material has a variety of metal

oxides with different shapes and sizes, which ensures more active sites due to more atoms on the surface and edges of the composite.

3.2. Optimization of the Adsorption Batch Method

The central composite design (CCD) matrix and the experimental data of Co are tabulated in Table 3; similar results were obtained for the other metals. The experimental results were statistically analyzed by means of analyses of variance (ANOVA), which is presented in a form of a Pareto chart (Figure 6). The parameters that were more influential on the adsorption process were pH, adsorbent mass and the interaction of pH and adsorbent mass. This can be noticed by passing the 95% confidence level. This implied that the parameters that are responsible for quantitative removal of target analytes in synthetic samples are pH and adsorbent mass.

Table 3. Box–Behnken design matrix and analytical response.

	pH	ET	MA	%Re
1	3.00	5.00	200	25.5
2	9.00	5.00	200	91.7
3	3.00	30.0	200	43.5
4	9.00	30.0	200	92.6
5	3.00	17.5	100	14.1
6	9.00	17.5	100	87.4
7	3.00	17.5	300	76.6
8	9.00	17.5	300	92.4
9	6.00	5.00	100	48.0
10	6.00	30.0	100	40.6
11	6.00	5.00	300	72.2
12	6.00	30.0	300	89.2
13	6.00	17.5	200	51.1
14	6.00	17.5	200	79.3
15	6.00	17.5	200	70.8

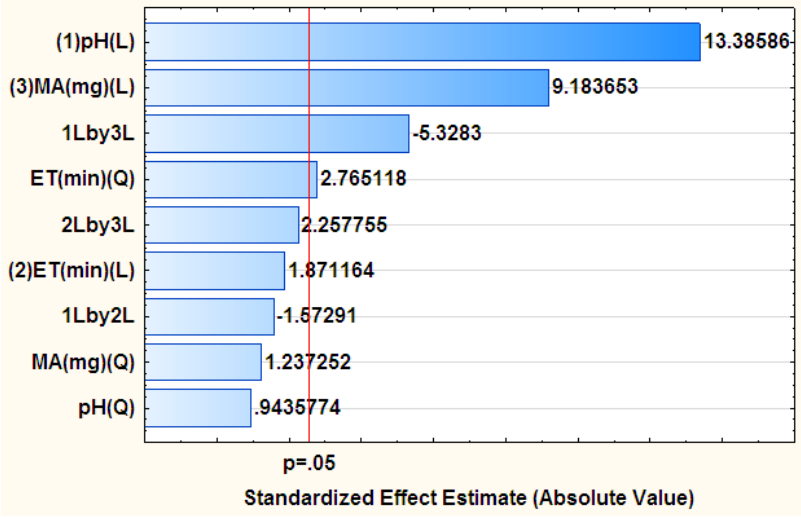

Figure 6. Chart of standardized estimated effects caused by investigated factors.

The quadratic models of the RSM was used to construct the response surface plots that were used to investigate the interactive effect of two independent factors and their interactions on the amount of trace metal adsorbed. The 3D plot of combined effect of pH with extraction time and adsorbent mass are shown in Figure 7. The maximum percentage recovery of the above 95% was obtained when pH was at the range of 8–8.3 and MA of 300–330 mg (Figure 7). Based on the RSM model the optimum condition were found to be MA 330 mg, sample pH 8.3 and extraction time of 24 min.

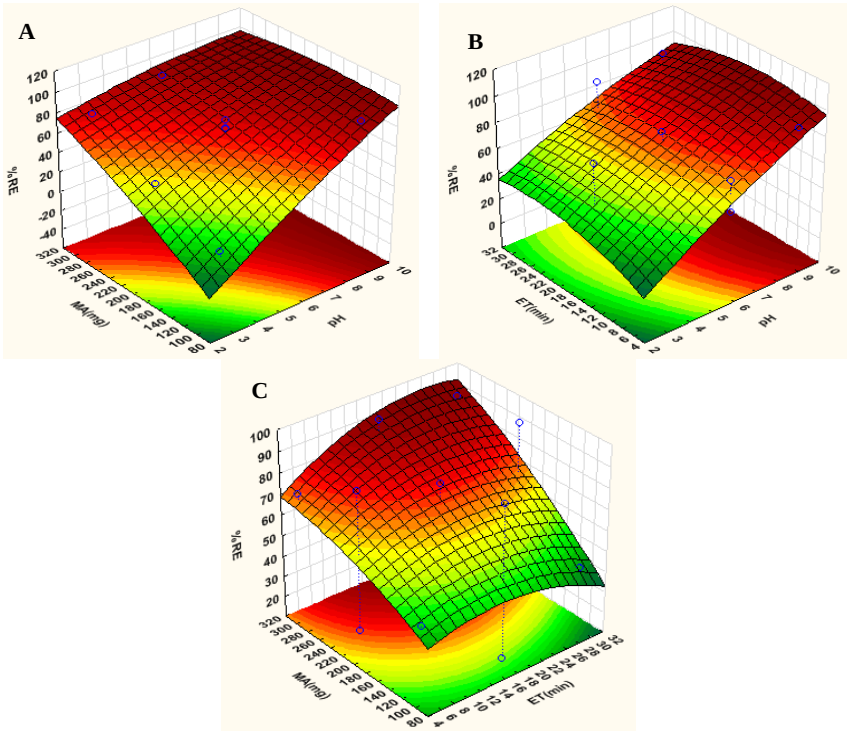

Figure 7. Response surface plot of combined effect of pH with extraction time and adsorbent mass, together with effect of adsorbent mass with extraction time on percentage recovery. (**A**) interaction between mass of adsorbent and sample pH, (**B**) interaction between extraction time and sample pH, (**C**) interaction between mass of adsorbent and extraction time

3.3. Confirmatory Experiments and Adsorption Capacity

The analytical data obtained from the RSM model under the optimized condition (pH 8.3, adsorbent mass of 330 mg and extraction time of 24 min) were validated by performing confirmatory experiments. According to the results given by the RSM model, the predicted response for sorption of Cr^{3+}, Cu^{2+}, Al^{3+}, Ba^{2+}, Zn^{2+}, Ni^{2+}, Mn^{2+}, Co^{2+}, and Ti^{3+} ranged from 95% to 97%. The experimental results ranged from 94% to 98% and these results were in close agreement with the predicted response.

3.4. Adsorption Kinetics

The adsorption kinetics of Cr^{3+}, Cu^{2+}, Al^{3+}, Ba^{2+}, Zn^{2+}, Ni^{2+}, Mn^{2+}, Co^{2+}, and Ti^{3+} were studied using the following kinetic models; pseudo-first order, pseudo-second order and the intra particle diffusion models. The equation for pseudo-first order is as follows:

$$\ln(q_e - q_t) = \ln q_e - k_1 t \tag{3}$$

where q_t is the amount of adsorbate, adsorbed (mg g^{-1}) at time t, q_e is equilibrium adsorption capacity (mg g^{-1}), k_1 is the rate constant (min^{-1}) The first order rate constant can be calculated from the intercept and slope of the plot [48,49]. Pseudo second order equation is as follows:

$$\frac{t}{q_t} = \frac{1}{k_2 {q_e}^2} + \frac{1}{q_e} t \tag{4}$$

where the equilibrium sorption capacity (q_e), q_t is the amount of adsorbate, adsorbed (mg g^{-1}) at time t and the second-order constant k_2 (g mg^{-1} min) (Table 4) can be determined experimentally from the slope and intercept of plot of t ${q_t}^{-1}$ versus t). Figure 8 shows the representative graphs for pseudo-second order equations. Kinetics were studied using the optimum parameters obtained from

the RSM method; pH 8.3, adsorbent mass of 330 mg and the concentration of 200 mg L^{-1}. It should be noted that for simplicity reasons only four graphs were presented. In addition, the initial sorption rate (h) and the half-adsorption times were calculated from Equations (5) and (6).

$$h = k_2 q_e^2 \tag{5}$$

$$t_{\frac{1}{2}} = \frac{1}{k_2 q_e} \tag{6}$$

Table 4. Kinetic parameters for pseudo-first order and second order model.

Pseudo-First Order				
Ions	q_{eexp}	k_1 (min^{-1})	q_e (mg g^{-1})	R^2
Al^{3+}	2.23	0.26	098	0.564
Ba^{2+}	6.60	0.15	1.20	0.606
Cr^{3+}	4.36	0.01	0.90	0.227
Cu^{2+}	7.20	0.02	3.40	0.389
Co^{2+}	6.65	0.23	1.30	0.899
Mn^{2+}	6.79	0.31	0.76	0.910
Ti^{3+}	3.00	0.05	1.40	0.874
Ni^{2+}	2.60	0.06	0.58	0.305
Zn^{2+}	5.06	0.01	0.72	0.824
Pseudo-Second Order				
Ions	q_e (mg g^{-1})	k_2 (g mg^{-1} min^{-1})	$t_{1/2}$ (min)	R^2
Al^{3+}	2.16	1.00	0.48	0.999
Ba^{2+}	6.80	0.03	4.90	0.918
Cr^{3+}	4.34	7.50	0.03	0.999
Cu^{2+}	7.35	0.42	0.32	0.999
Co^{2+}	7.04	0.02	8.71	0.800
Mn^{2+}	3.22	0.02	0.31	0.611
Ti^{3+}	2.86	0.13	2.63	0.998
Ni^{2+}	2.51	0.18	2.17	0.994
Zn^{2+}	5.10	0.69	0.28	0.999

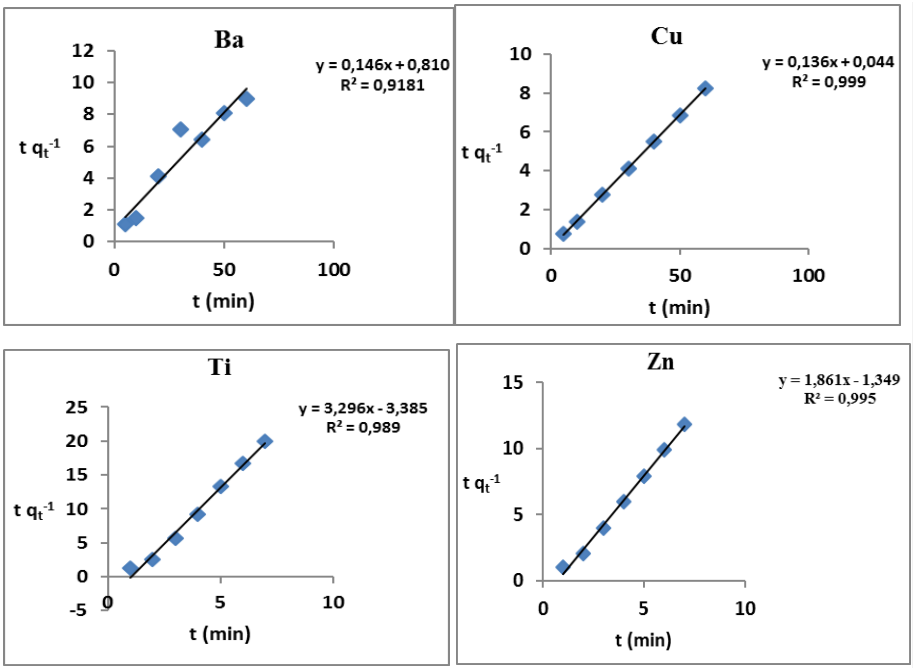

Figure 8. Graphs of pseudo-second order equation for Ba^{2+}, Cu^{2+}, Ti^{4+} and Zn^{2+}.

Table 4 shows results for pseudo-first and second-order. The correlation co-efficient (R^2) of pseudo-second order gives the best fit ($R^2 \geq 0.99$) for sorption of Cr^{3+}, Cu^{2+}, Al^{3+}, Ba^{2+}, Zn^{2+}, Ni^{2+}, Mn^{2+}, Co^{2+}, and Ti^{3+} onto Fe_2O_3-SiO_2-PAN together with $R^2 \geq 0.8$ for Co^{2+}. The pseudo-first order was followed by Mn^{2+} PTMs. The correlation co-efficient on this model was higher than the ones obtained in pseudo-first order model. Moreover, the q_e values that were calculated in pseudo-second order are in agreement with the experimental values obtained. This suggested that the adsorption process was chemisorption. Furthermore, the half-adsorption time is the time required in the removal of half of the amount of the analyte of interest at equilibrium [50]. The results show that the affinity was high between the adsorbent and metal ions; this can be seen through the short half-adsorption times achieved in most of the metals.

In order to get the information on the rate-limiting step, intraparticle diffusion was calculated and results were reported in Table 5. The step that limits the rate is either the boundary layer, which is the (film), or the intra particle (pore) diffusion of solute from the bulk solution to the adsorbent surface [51]. To investigate the chance of having intraparticle diffusion, Equation (7) was also used [51].

$$q_t = k_{id} t^{0.5} + C \quad (7)$$

Table 5. Kinetic parameters for intra particle diffusion.

Ions	k_{id} (g/mg min$^{1/2}$)	Q_e (mg g^{-1})	R^2
Al	0.05	2.07	0.987
Ba	1.13	1.16	0.832
Cr	0.03	4.43	0.753
Cu	0.32	6.85	0.515
Co	1.01	1.20	0.908
Mn	1.38	6.27	0.949
Ti	0.23	5.10	0.951
Ni	1.00	1.64	0.660
Zn	0.03	4.91	0.907

Adsorption capacity (q_t) is calculated at any time t, the k_{id} is the constant for intra particle diffusion (mg g^{-1} min$^{1/2}$) and C is the intercept. The experimental data of q_t versus $t^{1/2}$, was plotted and it was observed that a relatively good linear correlation existed between q_t and $t^{1/2}$. The intraparticle diffusion plots for adsorption of major and trace metals by the adsorbent showed that the regression lines did not pass the origin because C is non-zero. This implied that intraparticle diffusion was not the only rate-determining step [51–54]. This then suggested that both film diffusion and intraparticle diffusion influence the adsorption process. In addition, it is evident that stage 1 was influenced by electrostatic attraction between the external surface of the adsorbent the metal ions.

3.5. Application of Fe_2O_3-SiO_2-PAN in Real Samples

To evaluate the applicability of the optimized adsorption method, the synthesized adsorbent was used for the removal of PTMs from seawater collected from Durban, South Africa. Table 6, shows the analytical results before adsorption and after adsorption as well as percentage removal efficiencies. As seen from Table 6, the percentage removal efficiencies ranged from 98 to 99.9 suggesting that the Fe_2O_3-SiO_2-PAN was suitable for adsorptive removal of Al^{3+}, Ba^{2+}, Cr^{3+}, Cu^{2+}, Co^{2+}, Mn^{2+}, Ti^{3+}, Ni^{2+}, and Zn^{2+} from complex matrix such as seawater. It should be noted that the concentration of the metals adsorbed on the adsorbent were desorbed using 1.5 mol L^{-1} nitric acid. This was done in order to find the concentration after adsorption.

Table 6. Application of Fe_2O_3-SiO_2-PAN nanocomposite for removal of trace elements in real sample (n = 6 replicates).

Analytes	Initial Concentration (μg L^{-1})	Final Concentration (μg L^{-1}) [a]	%RE
Al^{3+}	203	2.79	98.6
Ba^{2+}	0.991	0.003	99.7
Cr^{3+}	0.270	0.002	99.2
Cu^{2+}	17.2	0.077	99.6
Co^{2+}	2.17	0.002	99.9
Mn^{2+}	1.49	0.002	99.9
Ti^{3+}	9.55	0.010	99.9
Ni^{2+}	65.3	1.36	98.0
Zn^{2+}	34.8	0.086	99.8

[a] Obtained by subtracting the concentration of metals after desorption from the intimal concentration.

The Fe_2O_3-SiO_2-PAN composite was comparable with previous adsorbents reported in the literature for the removal of trace elements from seawater [52–54]. Chelating resins were applied for the removal of Ni, Cu, Zn, Cd, Pb, Co, Cr, and Mn from seawater. Results showed that chelating resin was able to remove about 80% to 104% of the trace elements from seawater [55,56]. Therefore, the performance of Fe_2O_3-SiO_2-PAN composite was comparable with other studies and it removed trace metals from the seawater better than the reported adsorbents from the literature (Table 7).

Table 7. Comparison of heavy metal removal using other adsorbents.

Analytes	Adsorbents	Removal Efficiency (%)	Ref.
Pb (II), Cu (II), Cr (II), Cd (II)	Mabamboo activated carbon	99.9, 100, 96.4, 98.2	[57]
Zn (II)	Clinoptilolite	100	[58]
Ni (II)	Clinoptilolite	93.6	[59]
Cu (II), Cr (II), Ni (II)	Eryngium campestre	98.9, 98.2, 93.4	[60]
Fe, Pb, Cd, Cu, Ni	Fly ash	86.8, 76.1, 73.5, 98.6, 96.0	[61]
Cd, Cr, Mn, Cu, Ni, Pb, Zn, Fe	Aquatic plants	61.1, 69.2, 68.0, 79.1, 74.9, 62.1, 63.0, 81.2	[62]
Cr^{3+} Cu^{2+}, Al^{3+}, Ba^{2+}, Zn^{2+}, Ni^{2+}, Mn^{2+}, Co^{2+}, Ti^{3+}	Fe_2O_3-SiO_2-PAN	99.2, 99.6, 98.6, 99.7, 99.8, 98.0, 99.9, 99.9, 99.9	This work

4. Conclusions

In this study, the application on the Fe_2O_3-SiO_2-PAN adsorbent was executed for the removal of major and traces metals; Cr^{3+}, Cu^{2+}, Al^{3+}, Ba^{2+}, Zn^{2+}, Ni^{2+}, Mn^{2+}, Co^{2+}, and Ti^{3+} from synthetic brine and seawater samples. The prepared Fe_2O_3-SiO_2-PAN material was characterized by SEM, EDX, TEM, XRD, and BET surface area. The transmission electron image of the composite material shows a core-shell structured material that was formed on the surface of PAN. These results were further confirmed by EDX mapping that has densely covered Fe_2O_3-SiO_2 spheres. The removal of Cr^{3+}, Cu^{2+}, Al^{3+}, Ba^{2+}, Zn^{2+}, Ni^{2+}, Mn^{2+}, Co^{2+}, and Ti^{3+} was optimized using the Box-Behnken design matrix on pH, extraction time and adsorbent mass. Kinetic studies were investigated by fitting adsorption data on pseudo-first order, pseudo-second order and intraparticle diffusion. The adsorption data was best described by pseudo-second-order kinetic model and the intraparticle diffusion was not the rate-limiting step. The maximum percentage removal efficiency of metal ions Cr^{3+}, Cu^{2+}, Al^{3+}, Ba^{2+}, Zn^{2+}, Ni^{2+}, Mn^{2+}, Co^{2+}, and Ti^{3+} ion seawater samples ranged between 98% to 99.9%. These results demonstrated that Fe_2O_3-SiO_2-PAN composite is a suitable material for the removal of trace elements from seawater when compared with other reported studies.

Author Contributions: D.R.M., P.N., J.C.N. and P.N.N. formulated the research ideas; D.R.M. and P.N.N. designed the experiments; D.R.M. performed the experiment, collected and analyzed the data; D.R.M. wrote the first draft

of the manuscript, P.N. and P.N.N. review and edited the final version of the manuscript. P.N.N. supervised the project and assist with the funding support.

Funding: DAAD-NRF and NRF Thuthuka (grant no. 99270) funded this research.

Acknowledgments: The authors are grateful to the DAAD/NRF joint in-country scholarships and NRF Thuthuka (grant no. 99270) for assisting in this project financially and the University of Johannesburg (UJ), for providing infrastructure.

Conflicts of Interest: The authors declare no conflict of interest.

References

1. Khan, S.; Cao, Q.; Zheng, Y.M.; Huang, Y.Z.; Zhu, Y.G. Health risks of heavy metals in contaminated soils and food crops irrigated with wastewater in Beijing, China. *Environ. Pollut.* **2008**, *152*, 686–692. [CrossRef]
2. Gleick, P.H. Safe guarding our water making every drop count. *Sci. Am.* **2001**, *284*, 40–45. [CrossRef]
3. Zuehlke, S.; Duennbier, U.; Heberer, T. Investigation of the behaviour and metabolism of pharmaceutical residues during purification of contaminated ground water used for drinking water supply. *Chemosphere* **2007**, *69*, 1673–1680. [CrossRef]
4. Lyu, S.; Chen, W.; Zhang, W.; Fan, Y.; Jiao, W. Wastewater reclamation and reuse in China: opportunities and challenges. *J. Environ. Sci.* **2016**, *39*, 86–96. [CrossRef] [PubMed]
5. Bar-Zeev, E.; Berman-Frank, I.; Liberman, B.; Rahav, E.; Passow, U.; Berman, T. Transparent exopolymer particles: Potential agents for organic fouling and biofilm formation in desalination and water treatment plants. *Desalin. Water Treat.* **2009**, *3*, 136–142. [CrossRef]
6. Ali, Z.; Malik, R.N.; Qadir, A. Heavy metals distribution and risk assessment in soils affected by tannery effluents. *Chem. Ecol.* **2013**, *29*, 676–692. [CrossRef]
7. Nataraj, S.K.; Hosamani, K.M.; Aminabhavi, T.M. Potential application of an electrodialysis pilot plant containing ion-exchange membranes in chromium removal. *Desalination* **2007**, *217*, 181–190. [CrossRef]
8. Rodrigues, M.A.S.; Amado, F.D.R.; Xavier, J.L.N.; Streit, K.F.; Bernardes, A.M.; Ferreira, J.Z. Application of photoelectrochemical–electrodialysis treatment for the recovery and reuse of water from tannery effluents. *J. Clean. Prod.* **2008**, *16*, 605–611. [CrossRef]
9. Ku, Y.; Jung, I.L. Photocatalytic reduction of Cr (VI) in aqueous solutions by UV irradiation with the presence of titanium dioxide. *Water Res.* **2001**, *35*, 135–142. [CrossRef]
10. Fu, F.; Wang, Q. Removal of heavy metal ions from wastewaters: A review. *J. Environ. Manag.* **2011**, *92*, 407–418. [CrossRef]
11. Sohail, A.; Ali, S.I.; Khan, N.A.; Rao, R.A.K. Removal of chromium from wastewater by adsorption. *J. Environ. Pollut. Control.* **1999**, *2*, 27–31.
12. Shaaban, S.; Yahya, H. Detailed analysis of reverse osmosis systems in hot climate conditions. *Desalination* **2017**, *423*, 41–51. [CrossRef]
13. Li, Q.; Zhai, J.; Zhang, W.; Wang, M.; Zhou, J. Kinetic studies of adsorption of Pb (II), Cr (III) and Cu (II) from aqueous solution by sawdust and modified peanut husk. *J. Hazard. Mater.* **2007**, *141*, 163–167. [CrossRef] [PubMed]
14. Ma, Z.; Zhu, L.; Xing, Y.; Wu, Y.; Gao, Y. Facile synthesis of Mn–Co oxide with a hierarchical porous structure for heavy metal removal. *Mater. Lett.* **2013**, *108*, 261–263. [CrossRef]
15. Nyaba, L.; Matong, J.M.; Dimpe, K.M.; Nomngongo, P.N. Speciation of inorganic selenium in environmental samples after suspended dispersive solid phase microextraction combined with inductively coupled plasma spectrometric determination. *Talanta* **2016**, *159*, 174–180. [CrossRef] [PubMed]
16. Dimpe, K.M.; Nyaba, L.; Magoda, C.; Ngila, J.C.; Nomngongo, P.N. Synthesis, modification, characterization and application of AC@ Fe_2O_3@ MnO_2 composite for ultrasound assisted dispersive solid phase microextraction of refractory metals in environmental samples. *Chem. Eng. J.* **2017**, *308*, 169–176. [CrossRef]
17. Dimpe, K.M.; Ngila, J.C.; Nomngongo, P.N. Preparation and application of a tyre-based activated carbon solid phase extraction of heavy metals in wastewater samples. *Phys. Chem. Earth Parts A/B/C* **2018**, *105*, 161–169. [CrossRef]
18. Zeng, L. A method for preparing silica-containing iron (III) oxide adsorbents for arsenic removal. *Water Res.* **2003**, *37*, 4351–4358. [CrossRef]

19. Liu, B.; Wang, D.; Li, H.; Xu, Y.; Zhang, L. As (III) removal from aqueous solution using α-Fe_2O_3 impregnated chitosan beads with as (III) as imprinted ions. *Desalination* **2011**, *272*, 286–292. [CrossRef]
20. Mishra, A.K. *Nanomaterials for Water Remediation: Inorganic Oxide Materials*; Smithers Rapra: Shrewsbury, UK, 2016; Volume 2.
21. Ogoshi, T.; Chujo, Y. Synthesis of poly (vinylidene fluoride) (PVdF)/silica hybrids having interpenetrating polymer network structure by using crystallization between PVdF chains. *Part A J. Polym. Sci.* **2005**, *43*, 3543–3550. [CrossRef]
22. Ko, J.; Lee, J.; Yoo, B.; Ryu, J.; Sohn, D. Capillarity-induced selective ex-situ synthesis of metal–organic framework inside mesoporous nanotubes. *Micropor. Mesopor. Mater.* **2016**, *220*, 16–20. [CrossRef]
23. Wang, G.; Zhang, H.; Wang, J.; Ling, Z.; Qiu, J. In-situ synthesis of chemically active ZIF coordinated with electrospun fibrous film for heavy metal removal with a high flux. *Sep. Purif. Technol.* **2017**, *177*, 257–262. [CrossRef]
24. Lu, Q. *Synthesis of PDMS-Metal Oxide Hybrid Nanocomposites Using an In-Situ Sol-Gel Route*; Michigan Technological University: East Lansing, MI, USA, 2012.
25. Feng, Y.; Wang, Y.; Wang, Y.; Zhang, X.F.; Yao, J. In-situ gelation of sodium alginate supported on melamine sponge for efficient removal of copper ions. *J. Colloid Interf. Sci.* **2018**, *512*, 7–13. [CrossRef] [PubMed]
26. Mohamadi, Z.; Abdolmaleki, A. Heavy metal remediation via poly (3, 4-ethylene dioxythiophene) deposition onto neat and sulfonated nonwoven poly (ether sulfone). *J. Ind. Eng. Chem.* **2017**, *55*, 164–172. [CrossRef]
27. Park, H.S.; Kwak, S.H.; Mahardika, D.; Mameda, N.; Choo, K.H. Mixed metal oxide coated polymer beads for enhanced phosphorus removal from membrane bioreactor effluents. *Chem. Eng. J.* **2017**, *319*, 240–247. [CrossRef]
28. Roosta, M.; Ghaedi, M.; Daneshfar, A.; Sahraei, R. Experimental design based response surface methodology optimization of ultrasonic assisted adsorption of safaranin O by tin sulfide nanoparticle loaded on activated carbon. *Spectrochim. Acta A Mol. Biomol. Spectrosc.* **2014**, *122*, 223–231. [CrossRef]
29. Hamdaoui, O.; Chiha, M.; Naffrechoux, E. Ultrasound-assisted removal of malachite green from aqueous solution by dead pine needles. *Ultrason. Sonochem.* **2008**, *15*, 799–807. [CrossRef]
30. Asfaram, A.; Ghaedi, M.; Hajati, S.; Goudarzi, A.; Bazrafshan, A.A. Simultaneous ultrasound-assisted ternary adsorption of dyes onto copper-doped zinc sulfide nanoparticles loaded on activated carbon: Optimization by response surface methodology. *Spectrochim. Acta A Mol. Biomol. Spectrosc.* **2015**, *145*, 203–212. [CrossRef] [PubMed]
31. Dos Santos Fernandes, J.P.; Carvalho, B.S.; Luchez, C.V.; Politi, M.J.; Brandt, C.A. Optimization of the ultrasound-assisted synthesis of allyl 1-naphthyl ether using response surface methodology. *Ultrason. Sonochem.* **2011**, *18*, 489–493. [CrossRef]
32. Xu, P.; Zeng, G.M.; Huang, D.L.; Feng, C.L.; Hu, S.; Zhao, M.H.; Liu, Z.F. Use of iron oxide nanomaterials in wastewater treatment: A review. *Sci. Total Environ.* **2012**, *424*, 1–10. [CrossRef]
33. Hua, M.; Zhang, S.; Pan, B.; Zhang, W.; Lv, L.; Zhang, Q. Heavy metal removal from water/wastewater by nanosized metal oxides: A review. *J. Hazard. Mater.* **2012**, *211–212*, 317–331. [CrossRef]
34. Vojoudi, H.; Badiei, A.; Bahar, S.; Ziarani, G.M.; Faridbod, F.; Ganjali, M.R. A new nano-sorbent for fast and efficient removal of heavy metals from aqueous solutions based on modification of magnetic mesoporous silica nanospheres. *J. Magn. Magn. Mater.* **2017**, *441*, 193–203. [CrossRef]
35. Laurent, S.; Forge, D.; Port, M.; Roch, A.; Robic, C.; Vander Elst, L.; Muller, R.N. Magnetic iron oxide nanoparticles: Synthesis, stabilization, vectorization, physicochemical characterizations, and biological applications. *Chem. Rev.* **2008**, *108*, 2064–2110. [CrossRef]
36. Bai, L.; Hu, H.; Fu, W.; Wan, J.; Cheng, X.; Zhuge, L.; Chen, Q. Synthesis of a novel silica-supported dithiocarbamate adsorbent and its properties for the removal of heavy metal ions. *J. Hazard. Mater.* **2011**, *195*, 261–275. [CrossRef]
37. Liu, J.; Ma, S.; Zang, L. Preparation and characterization of ammonium-functionalized silica nanoparticle as a new adsorbent to remove methyl orange from aqueous solution. *Appl. Surf. Sci.* **2013**, *265*, 393–398. [CrossRef]
38. Ramutshatsha, D.; Ngila, J.C.; Ndungu, P.G.; Nomngongo, P.N. Simultaneous removal of Na, Ca, K and Mg from synthetic brine and seawater using Fe_2O_3-SiO_2 mixed oxide nanostructures: Kinetics and isotherms studies. *Desalin. Water Treat.* **2018**, *104*, 206–216. [CrossRef]

39. İnan, S.; Altaş, S. Preparation of zirconium–manganese oxide/polyacrylonitrile (Zr–Mn oxide/PAN) composite spheres and the investigation of Sr (II) sorption by experimental design. *Chem. Eng. J.* **2011**, *168*, 1263–1271. [CrossRef]
40. Scharnagl, N.; Buschatz, H. Polyacrylonitrile (PAN) membranes for ultra-and microfiltration. *Desalination* **2001**, *139*, 191–198. [CrossRef]
41. Almasian, A.; Najafi, F.; Maleknia, L. Mesoporous MgO/PPG hybrid nanofibers: Synthesis, optimization, characterization and heavy metal removal property. *New J. Chem.* **2018**, *42*, 2013–2029. [CrossRef]
42. Zhang, H.; Nie, H.; Yu, D.; Wu, C.; Zhang, Y.; White, C.J.B.; Zhu, L. Surface modification of electrospunpolyacrylonitrile nanofiber towards developing an affinity membrane for bromelain adsorption. *Desalination* **2010**, *256*, 141–147. [CrossRef]
43. Panda, N.; Sahoo, H.; Mohapata, S. Decolourization of methyl orange using Fenton-like mesoporous Fe_2O_3–SiO_2 composite. *J. Hazard. Mater.* **2011**, *185*, 359–365. [CrossRef] [PubMed]
44. Bhaumik, M.; Maity, A.; Srinivasu, V.V.; Onyango, M.S. Enhanced removal of Cr (VI) from aqueous solution using polypyrrole/Fe_3O_4 magnetic nanocomposite. *J. Hazard. Mater.* **2011**, *190*, 381–390. [CrossRef]
45. Setshedi, K.Z.; Bhaumik, M.; Onyango, M.S.; Maity, A. High-performance towards Cr (VI) removal using multi-active sites of polypyrrole–graphene oxide nanocomposites: Batch and column studies. *Chem. Eng. J.* **2015**, *262*, 921–931. [CrossRef]
46. Teo, H.T.; Siah, W.R.; Yuliati, L. Enhanced adsorption of acetylsalicylic acid over hydrothermally synthesized iron oxide-mesoporous silica MCM-41 composites. *J. Taiwan Inst. Chem. Eng.* **2016**, *65*, 591–598. [CrossRef]
47. Munonde, T.S.; Maxakato, N.W.; Nomngongo, P.N. Preconcentration and speciation of chromium species using ICP-OES after ultrasound-assisted magnetic solid phase extraction with an amino-modified magnetic nanocomposite prepared from Fe_3O_4, MnO_2 and Al_2O_3. *Mikrochim. Acta* **2017**, *184*, 1223–1232. [CrossRef]
48. Naushad, M. Surfactant-assisted nano-composite cation exchanger: Development, characterization and applications for the removal of toxic Pb^{2+} from aqueous medium. *Chem. Eng. J.* **2014**, *235*, 100–108. [CrossRef]
49. Lagergren, S. Zurtheorie der sogenannten adsorption gelosterstoffe, Kungligasvenskavetenskapsakademiens. *Handlingar* **1898**, *24*, 1–39.
50. Nomngongo, P.N.; Ngila, J.C.; Msagati, T.A.; Moodley, B. Kinetics and equilibrium studies for the removal of cobalt, manganese, and silver in ethanol using Dowex 50W-x8 cation exchange resin. *Sep. Sci. Technol.* **2014**, *49*, 1848–1859. [CrossRef]
51. Weber, W.J.; Morris, J.C. Equilibria and capacities for adsorption on carbon. *J. Sanit. Eng. Div.* **1964**, *90*, 79–108.
52. Su, S.; Che, R.; Liu, Q.; Liu, J.; Zhang, H.; Li, R.; Wang, J. ZeoliticImidazolate Framework-67: A promising candidate for recovery of uranium (VI) from seawater. *Colloids Surf. A Physicochem. Eng. Asp.* **2018**, *547*, 73–80. [CrossRef]
53. Hong, H.J.; Kim, B.G.; Ryu, J.; Park, I.S.; Chung, K.S.; Lee, S.M.; Ryu, T. Preparation of highly stable zeolite-alginate foam composite for strontium (90 Sr) removal from seawater and evaluation of Sr adsorption performance. *J. Environ. Manag.* **2018**, *205*, 192–200. [CrossRef]
54. Demey, H.; Vincent, T.; Ruiz, M.; Nogueras, M.; Sastre, A.M.; Guibal, E. Boron recovery from seawater with a new low-cost adsorbent material. *Chem. Eng. J.* **2014**, *254*, 463–471. [CrossRef]
55. AlSuhaimi, A.O.; AlRadaddi, S.M.; Ali, A.K.A.S.; Shraim, A.M.; AlRadaddi, T.S. Silica-based chelating resin bearing dual 8-Hydroxyquinoline moieties and its applications for solid phase extraction of trace metals from seawater prior to their analysis by ICP-MS. *Arab. J. Chem.* **2017**, *12*, 360–369. [CrossRef]
56. Trujillo, I.S.; Alonso, E.V.; de Torres, A.G.; Pavón, J.M.C. Development of a solid phase extraction method for the multielement determination of trace metals in natural waters including sea-water by FI-ICP-MS. *Microchem. J.* **2012**, *101*, 87–94. [CrossRef]
57. Lo, S.F.; Wang, S.Y.; Tsai, M.J.; Lin, L.D. Adsorption capacity and removal efficiency of heavy metal ions by Moso and Ma bamboo activated carbons. *Chem. Eng. Res. Des.* **2012**, *90*, 1397–1406. [CrossRef]
58. Athanasiadis, K.; Helmreich, B. Influence of chemical conditioning on the ion exchange capacity and on kinetic of zinc uptake by clinoptilolite. *Water Res.* **2005**, *39*, 1527–1532. [CrossRef]
59. Argun, M.E. Use of clinoptilolite for the removal of nickel ions from water: Kinetics and thermodynamics. *J. Hazard. Mater.* **2008**, *150*, 587–595. [CrossRef]
60. Vaseghi, Z.; Nematollahzadeh, A.; Tavakoli, O. Plant-mediated Cu/Cr/Ni nanoparticle formation strategy for simultaneously separation of the mixed ions from aqueous solution. *J. Taiwan Inst. Chem. Eng.* **2019**, *96*, 148–159. [CrossRef]

61. Hegazi, H.A. Removal of heavy metals from wastewater using agricultural and industrial wastes as adsorbents. *HBRC J.* **2013**, *9*, 276–282. [CrossRef]
62. Syukor, A.A.; Sulaiman, S.; Siddique, M.N.I.; Zularisam, A.W.; Said, M.I.M. Integration of phytogreen for heavy metal removal from wastewater. *J. Clean. Prod.* **2016**, *112*, 3124–3131. [CrossRef]